RSC Advances

PAPER

View Article Online
View Journal | View Issue

Cite this: *RSC Adv.*, 2021, **11**, 34402

Reversible CO_2 storage and efficient separation using Ca decorated porphyrin-like porous $C_{24}N_{24}$ fullerene: a DFT study†

Mehdi D. Esrafili *[a] and Sharieh Hosseini[b]

The search for novel materials for effective storage and separation of CO_2 molecules is a critical issue for eliminating or lowering this harmful greenhouse gas. In this paper, we investigate the potential application of a porphyrin-like porous fullerene ($C_{24}N_{24}$) as a promising material for CO_2 storage and separation using thorough density functional theory calculations. The results show that CO_2 is physisorbed on bare $C_{24}N_{24}$, implying that this material cannot be used for efficient CO_2 storage. Coating $C_{24}N_{24}$ with Ca atoms, on the other hand, can greatly improve the adsorption strength of CO_2 molecules due to polarization and charge-transfer effects. Furthermore, the average adsorption energy for each of the maximum 24 absorbed CO_2 molecules on the fully decorated $Ca_6C_{24}N_{24}$ fullerene is −0.40 eV, which fulfills the requirement needed for efficient CO_2 storage (−0.40 to −0.80 eV). The Ca coated $C_{24}N_{24}$ fullerene also have a strong potential for CO_2 separation from CO_2/H_2, CO_2/CH_4, and CO_2/N_2 mixtures.

Received 3rd August 2021
Accepted 13th October 2021

DOI: 10.1039/d1ra05888f

rsc.li/rsc-advances

1. Introduction

The discovery of fullerene C_{60} in 1985 (ref. 1) and subsequently of related materials like carbon nanotubes (CNTs)[2,3] and graphene[4,5] marked the beginning of a new era in carbon chemistry. Numerous potential applications of these nanosized carbon structures have been proposed, including hydrogen storage,[6–8] microelectronics,[9,10] and smart and novel composites.[11,12] These structures are also well suited for use as a support in heterogeneous catalysis due to their huge specific area.[13–15] The ability to tune the electronic and surface properties of carbon-based nanomaterials by introducing defects or heteroatoms has shed light on their potential use in sensors and energy technologies.[16–19] Theoretical calculations[20–22] and experimental investigations,[23,24] for example, have demonstrated that N atoms may be effectively incorporated in different carbon materials, tailoring their chemical and electronic characteristics. Although the loading of metal atoms on pure carbon nanomaterials usually results in aggregation due to weak metal–surface interactions, previous studies have demonstrated that the doping of N atoms can substantially enhance metal atom dispersion on these systems due to polarized C–N bonds.[22,25,26] Furthermore, a variety of porous N-rich carbon nanomaterials including graphitic carbon nitride (g-C_3N_4)[27,28] and porphyrin like graphene[29–31] or CNTs[32,33] have been prepared using different experimental methods. There is also evidence that N-rich porous carbon fullerenes can provide as active sites for metal atoms by forming strong metal–N covalent bonds.[34,35] $C_{24}N_{24}$, a truncated N-doped C_{60} fullerene, is the best example of such systems. This fullerene comprises six porphyrin-like N_4 cavities, each of which is made up of eight *s*-triazine rings linked together by C–C bonds.[36] Metal atoms may be efficiently trapped by these N_4 cavities, and the clustering problem of metal atoms is therefore avoided due to the strong metal–N interactions. In fact, the potential of such single atom catalysts (SACs) based on porous $C_{24}N_{24}$ has been found in a variety of chemical processes, including N_2O[37] or O_2 reduction,[38] and CO oxidation.[39]

Growing energy demands, along with the ongoing use of fossil fuels in vehicles and power plants, has resulted in serious environmental issues such as emission of greenhouse gases and air pollution. CO_2 is the most dangerous and prevalent greenhouse gas that has the potential to contribute to global warming and climate change.[40] Given these facts, several strategies have been explored in order to lower the level of CO_2 in the atmosphere. The most essential and straightforward method is to switch from fossil fuels to cleaner ones, such as natural gas.[41] Natural gas emits less CO_2 than other fossil fuels and is inexpensive and widely available. Landfills are a source of natural gas, but they can also contain significant amounts of CO_2. As a result, separating CO_2 from methane is a critical issue.[42] Hydrogen is a clean fuel that emits no CO_2 when burned,

[a]*Department of Chemistry, Faculty of Basic Sciences, University of Maragheh, P.O. Box 55136-553, Maragheh, Iran. E-mail: esrafili@maragheh.ac.ir; Fax: +98 4212276060; Tel: +98 4212237955*

[b]*Department of Chemistry, Faculty of Pharmaceutical Chemistry, Tehran Medical Sciences, Islamic Azad University, Tehran, Iran*

† Electronic supplementary information (ESI) available. See DOI: 10.1039/d1ra05888f

therefore the separation of CO_2 from H_2 is also important for practical purposes.[43] Another alternative is to look into potential CO_2 storage, capture, or transformation technologies.[44–47] Recently, there has been a lot of interest in the capture and storage of CO_2 on porous materials with high selectivity and capacity, such as zeolites[48,49] and covalent organic frameworks.[50,51] However, for efficient CO_2 storage, these materials generally require either low temperature or high pressure. As a result, it is critical to investigate novel materials capable of capturing CO_2 under normal conditions.

CO_2 mostly acts as a Lewis acid in supramolecular chemistry by accepting electrons from the host material, but there is evidence that it may also serve as a Lewis base due to the existence of O lone-pair electrons.[52] Because N-doped carbon nanostructures such as graphene, fullerenes, and CNTs are electron-rich materials, they may initially be assumed to be effective CO_2 adsorbents. However, previous DFT calculations[53,54] have shown that CO_2 is generally weakly physisorbed on these surfaces due to lack of a permanent dipole moment. Some effective ways for solving the problem have been proposed, such as coating these substrates with atoms such as Ca,[55,56] using an external electric field[57,58] and charge regulation of the substrate.[59] For instance, prior studies have shown that coating carbon fullerenes or their analogues[60,61] with Ca atoms can significantly increase the CO_2 storage capacity of these systems. The current work aims to investigate CO_2 adsorption and storage on bare and Ca coated $C_{24}N_{24}$ fullerenes using density functional theory (DFT) calculations. It appears that the existence of N_4 cavities in $C_{24}N_{24}$ not only provides active sites for Ca atoms to be located, but also induces a significant positive charge on the Ca, which improves adsorption abilities towards CO_2 molecules. Surprisingly, the addition of Ca atoms causes $C_{24}N_{24}$ to behave as a Lewis acid when it interacts with CO_2. Furthermore, the capability of Ca coated $C_{24}N_{24}$ fullerenes to separate CO_2 from various gas mixtures (CO_2/N_2, CO_2/CH_4, CO_2/H_2) is investigated.

2. Computational details

The Perdew–Burke–Ernzerhof (PBE)[62] formalism within the DMol^3 (ref. 63 and 64) was used to execute spin polarized DFT computations. To get reliable results, an all-electron double-numeric atomic orbital basis set (DNP) was used, which was augmented by d-polarization functions. Fully optimized structures were obtained without the application of symmetry constraints. In this study, the Hirshfeld analysis was used to provide atomic charges and charge-transfer values. The Grimme's PBE + D2 (ref. 65) method was used to account for weak van der Waals interactions. A convergence tolerance of 1×10^{-5} Ha, 0.001 Ha Å^{-1}, and 0.005 Å was used for energy change, maximum force, and maximum displacement, respectively. The porous $C_{24}N_{24}$ was produced as follows. First, two carbon atoms of C_{60} fullerene linking the two five-membered rings were deleted, and then four carbon atoms in the closest nearby places were replaced with N atoms. For the computations, a periodic cubic box with dimensions $a = b = c = 30$ Å was used, the Brillouin zone sampling by the Γ point.

The following equation was used to calculate the adsorption energy per adsorbed CO_2 molecule $E_{ads}(CO_2)$, on Ca coated $C_{24}N_{24}$ clusters:

$$E_{ads}(CO_2) = 1/n[E_{complex} - E_{cluster} - nE_{CO_2}] \quad (1)$$

where n is the number of adsorbed CO_2 molecules, $E_{complex}$ represents the energy of CO_2 adsorbed on the Ca coated $C_{24}N_{24}$ structure, $E_{cluster}$ represents the energy of Ca coated $C_{24}N_{24}$, and E_{CO_2} is the energy of a free CO_2 molecule.

The adsorption of CO_2 is supposed to cause a mutual redistribution of electron density on $C_{24}N_{24}$ as well as on CO_2. To demonstrate this, we used the following equation to obtain electron density difference (EDD) maps:

$$EDD = \rho(CO_2@C_{24}N_{24}) - \rho(CO_2) - \rho(C_{24}N_{24}) \quad (2)$$

in which $\rho(CO_2@C_{24}N_{24})$, $\rho(CO_2)$ and $\rho(C_{24}N_{24})$ are the electron densities of CO_2 adsorbed on $C_{24}N_{24}$, free CO_2 and $C_{24}N_{24}$, respectively.

The Bader's atoms in molecules (AIM)[66] theory was utilized to investigate the nature of the interaction between CO_2 molecules and Ca coated $C_{24}N_{24}$ fullerenes. In summary, the AIM theory is based on the topology of the electron density. In the AIM theory, the nature of the interaction between two interacting atoms is characterized by analyzing electron density (ρ_{BCP}) and its Laplacian ($\nabla^2\rho_{BCP}$) at a specific point called the bond critical point (BCP), where the gradient of the electron density is zero.[66] For a closed-shell or noncovalent interaction, such as most weak and moderate hydrogen bonds, the electron density at the BCPs is low and the Laplacian is positive. For a chemical bonding, on the other hand, the ρ_{BCP} is big and its $\nabla^2\rho_{BCP}$ is negative at the corresponding BCP. In the AIM, another useful indicator for analyzing the nature of the interaction is the total electron energy density (H_{BCP}), whose sign, together with the sign of $\nabla^2\rho_{BCP}$, may indicate whether the interaction is electrostatic or covalent. That is, $\nabla^2\rho_{BCP} < 0$ and $H_{BCP} < 0$ for strong covalent bonds; $\nabla^2\rho_{BCP} > 0$ and $H_{BCP} > 0$ for electrostatic interactions; and $\nabla^2\rho_{BCP} > 0$ and $H_{BCP} < 0$ for partially covalent interactions.[67] To perform the AIM analysis, wavefunctions were first generated at the PBEPBE/6-31G* level using the PBE/DNP optimized geometries by means of Gaussian 09 suite of program.[68] The AIM2000 (ref. 69) was then used for topology analysis of the electron densities.

3. Results and discussion

3.1. Bare $C_{24}N_{24}$

Fig. 1a depicts the optimized structure of bare $C_{24}N_{24}$ cluster. It was prepared *via* truncated N-doping of C_{60} fullerene in accordance with ref. 37. As can be seen, $C_{24}N_{24}$ is made up of six porphyrine-like N_4 cavities, each of which is composed of eight *s*-triazine rings connected by C–C bonds. The optimized C–N and C–C bond lengths in $C_{24}N_{24}$ are 1.34 and 1.55 Å, respectively, which are consistent with other DFT studies.[36,38,70] The Hirshfeld charges on the N and C atoms are determined to be −0.12 and +0.12|*e*|, respectively, suggesting that $C_{24}N_{24}$ has

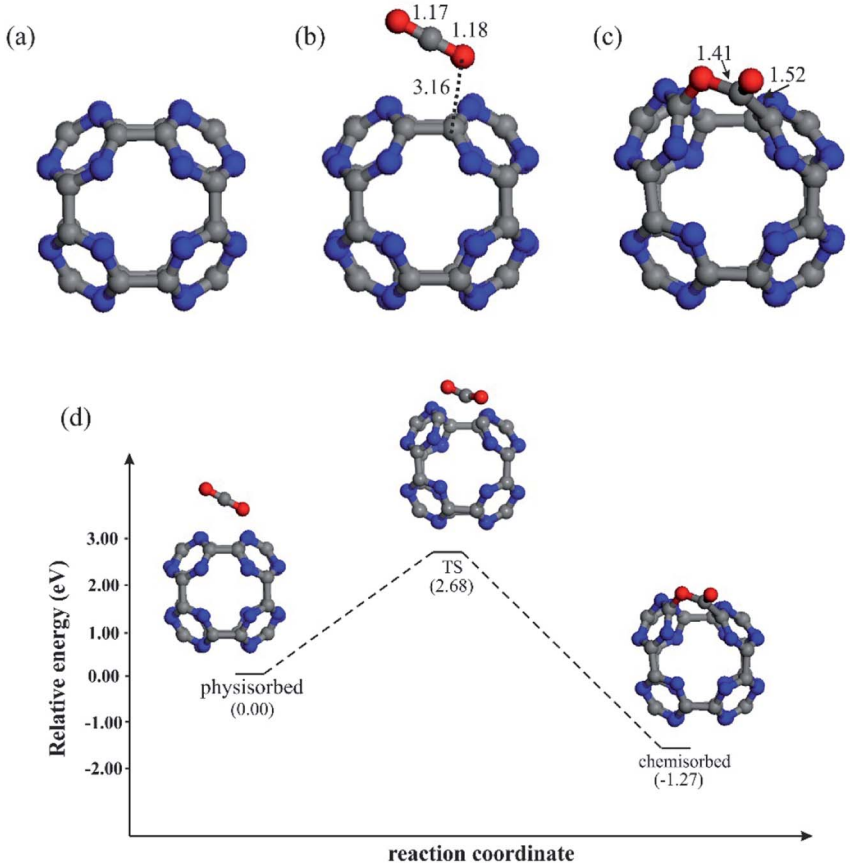

Fig. 1 (a) The optimized structure of $C_{24}N_{24}$, (b) physisorbed structure of CO_2 on $C_{24}N_{24}$, (c) chemisorbed structure of CO_2 on $C_{24}N_{24}$ and (d) the energy map for the physisorbed-to-chemisorbed transformation of CO_2 on of $C_{24}N_{24}$. The color code of the atoms: O (red); C (gray); N (blue). The values on the optimized structures are bond distances (in Å).

a partially polarized C–N bonds. The formation energy (E_{form}) of $C_{24}N_{24}$ is determined to be about −6.0 eV, which is defined as $E_{form} = 1/48[E_{C_{24}N_{24}} - 24E_C - 24E_N]$, where $E_{C_{24}N_{24}}$ is the energy of $C_{24}N_{24}$ and E_C and E_N are the energies of a single C and N atom, respectively. This negative number, which agrees satisfactory with that reported by Srinivasu and Ghosh,[36] suggests that the formation of $C_{24}N_{24}$ is a thermodynamically favorable process.

To assess the CO_2 storage capability of bare $C_{24}N_{24}$, we first study the adsorption properties of a single CO_2 molecule on this system. Fig. 1b and c depict the most stable geometries of a CO_2 molecule adsorbed on $C_{24}N_{24}$. Consistent with other DFT studies,[71,72] two stable configurations were located for CO_2, namely the physisorbed and chemisorbed. In the physisorbed configuration, CO_2 is nearly parallel to the C–C bond of fullerene, and the minimum binding distance between CO_2 and $C_{24}N_{24}$ is 3.16 Å. The adsorption energy (E_{ads}) is −0.14 eV, which is much smaller than the minimum target for an efficient storage of CO_2 molecule (−0.40 eV).[73] Meanwhile, this low adsorption energy and negligible charge transfer ($0.02|e|$) owing to CO_2 adsorption suggest that bare $C_{24}N_{24}$ cannot efficiently adsorb CO_2. Our DFT results, on the other hand, show that CO_2 may be strongly chemisorbed on the $C_{24}N_{24}$, with an adsorption energy of −1.42 eV. This E_{ads} value is much larger than that of on the B_{80} (ref. 71) and B_{40} (ref. 72) clusters, suggesting that CO_2 is strongly bound to the $C_{24}N_{24}$. However, unlike the physisorbed structure, the formation of the chemisorbed structure on $C_{24}N_{24}$ requires the passing of an activation barrier. To investigate the mechanism of CO_2 chemisorption, the potential energy profile for the physisorption-to-chemisorption conversion of CO_2 molecule is investigated (Fig. 1d). Our results demonstrate that, while the conversion of physisorbed-to-chemisorbed configuration on $C_{24}N_{24}$ is exothermic, a significant activation barrier must be overcome for this process to occur. As a result, $C_{24}N_{24}$ cannot be used as an efficient CO_2 storage material at room temperature.

3.2. Ca coated $C_{24}N_{24}$

The interaction of a Ca atom with $C_{24}N_{24}$ is then considered. The most stable atomic configuration for a Ca atom adsorbed on the $C_{24}N_{24}$ is shown in Fig. 2a. The Ca atom, like transition metals,[38,74–76] prefers to reside in the N_4 cavity, with an E_{ads} value of −6.85 eV. The distance between the Ca atom and the adjacent N atoms is 2.33 Å. Furthermore, the presence of the Ca atom alters slightly the geometry of $C_{24}N_{24}$, as evidenced by the elongation of adjacent C–N bond lengths from 1.34 Å in bare $C_{24}N_{24}$ to 1.38 Å in $CaC_{24}N_{24}$. The decorated Ca atom is positively charged by $0.74|e|$, whereas the nitrogen atoms around it are negatively charged by $0.17|e|$, according to the Hirshfeld

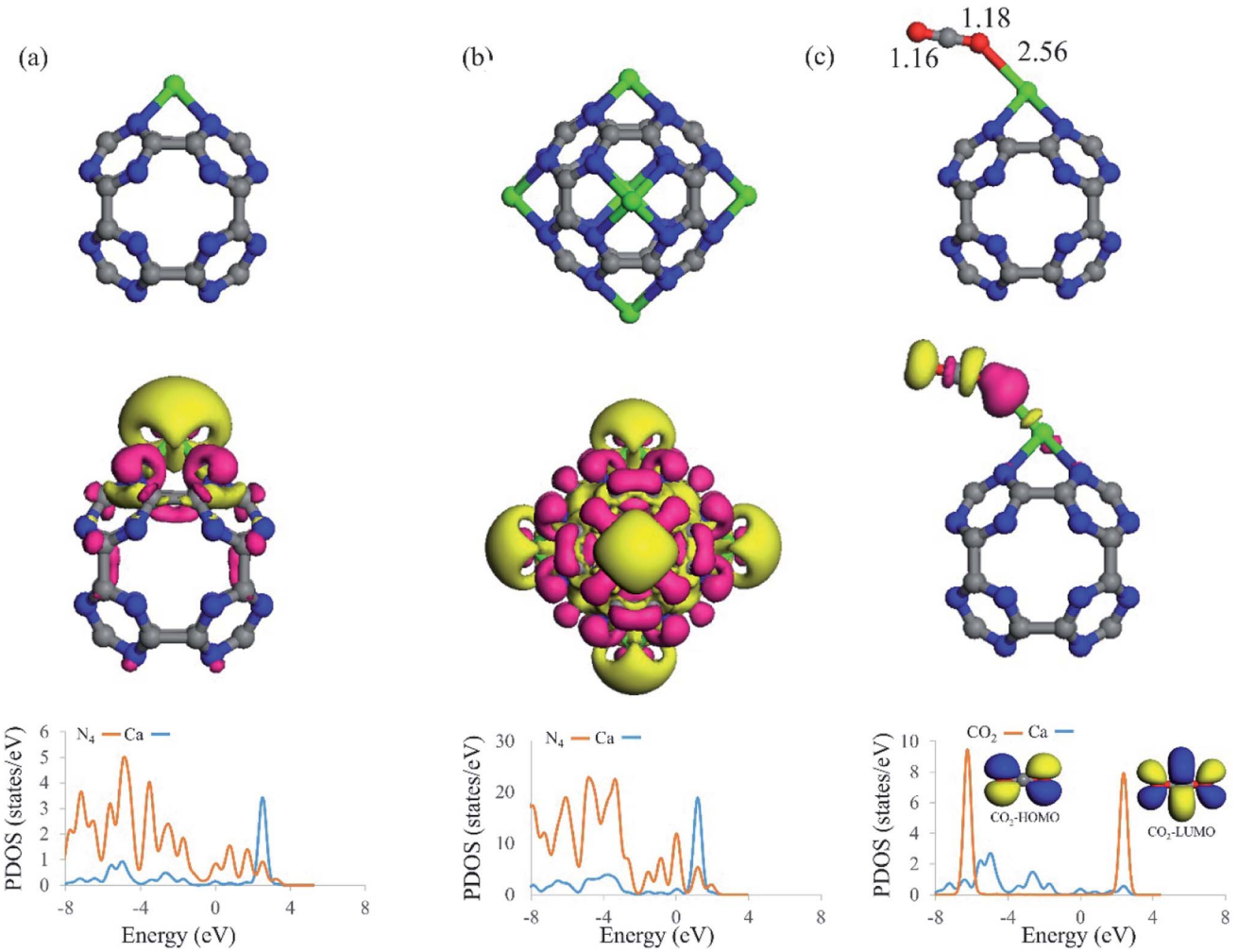

Fig. 2 The optimized structure (above), corresponding EDD (middle, isovalue = 0.002 au) and the PDOS plots of (a) $CaC_{24}N_{24}$, (b) $Ca_6C_{24}N_{24}$ and (c) CO_2@$CaC_{24}N_{24}$. In the EDD plots, the electron gain and loss regions are denoted by pink and yellow colors, respectively. The Fermi level in the PDOS plots is set to zero. The color code of the atoms: Ca (green); O (red); C (gray); N (blue).

analysis. Due to Coulomb interactions, such a large charge transfer might be helpful to the stability of Ca atoms coated on $C_{24}N_{24}$. Furthermore, the significant localization of positive charge on the Ca atom may generate an electric field that polarizes the adsorbed CO_2 molecules, fascinating their adsorption. Fig. 2a also shows the associated EDD map, which is used to evaluate the degree of electron density redistribution induced by Ca adsorption. A significant electron density loss region emerges on the Ca atom as a result of the formation of the $CaC_{24}N_{24}$ complex, demonstrating the ability of this site to interact with the electron donating species. Meanwhile, electron density gain regions exist between the Ca and N atoms, confirming the formation of Ca–N covalent bonds in $CaC_{24}N_{24}$. The PDOS analysis in Fig. 2a, on the other hand, clearly shows that the electronic states of the Ca and its surrounding N atoms are substantially mixed above and below the Fermi level ($E = 0$). As a consequence, it is reasonable to conclude that charge-transfer effects, in addition to electrostatic and polarization interactions between Ca and N atoms, are driving forces in the formation of Ca–N bonds.

Fig. 1b shows the optimized structure of $Ca_6C_{24}N_{24}$ cluster, in which one Ca atom is placed on each N_4 cavity of $C_{24}N_{24}$. According to the calculations, the E_{ads} value per Ca atom in this system is −6.31 eV, which is less negative than that of $CaC_{24}N_{24}$, partly due to repulsion between the decorated Ca atoms. To clarify this, we removed $C_{24}N_{24}$ from $Ca_6C_{24}N_{24}$ and calculated the single-point energy of the remaining 6 Ca atoms. The average energy of the leftover 6 Ca atoms was determined to be 0.17 eV higher than the energy of a single Ca atom. On the other hand, as the number of the incorporated Ca atoms increases, it is natural to expect that the tendency of the cluster to accept electrons from the Ca atoms decreases. Hence, we believe that the lower average E_{ads} value of Ca atom compared to the E_{ads} value of $CaC_{24}N_{24}$ can be attributed to the latter two effects. This is supported by the Hirshfeld analysis, which shows that the average positive charge (0.64|e|) on the Ca atoms in $Ca_6C_{24}N_{24}$ is likewise less than the positive charge on the Ca atom in $CaC_{24}N_{24}$ (0.74|e|). Furthermore, the significant electron density shifts caused by Ca atoms adsorption on $C_{24}N_{24}$, as well as the strong coupling between the electronic states in Fig. 2b,

demonstrate that the Ca atoms are firmly bonded to the N atoms. As previously stated, the aggregation of coated Ca atoms may have a detrimental influence on CO_2 storage. To address this issue, we compared the average E_{ads} value of Ca atoms in $Ca_6C_{24}N_{24}$ to the cohesive energy of bulk Ca (−1.82 eV per Ca atom). It is revealed that, due to higher average E_{ads}, Ca atoms are firmly adsorbed on the N_4 cavities of $C_{24}N_{24}$, avoiding the formation of Ca clusters on this cluster. This is also seen in Fig. 3, where the formation of a Ca_6 cluster on $C_{24}N_{24}$ from $Ca_6C_{24}N_{24}$ is highly endothermic by 23.01 eV. Such a result can be validated further by *ab initio* molecular dynamic (MD) simulations. The final structure of $Ca_6C_{24}N_{24}$ following MD simulation at 500 K and for 2ps is depicted in Fig. S1 of the ESI.† The Ca atoms are clearly shown to be still located on the hollow sites of $C_{24}N_{24}$, and therefore the $Ca_6C_{24}N_{24}$ stays stable after the MD simulations. As a result, $Ca_6C_{24}N_{24}$ is stable enough to be employed as a CO_2 storage material at ambient or even high temperatures.

We investigated the adsorption of CO_2 molecules on Ca coated clusters to examine if the Ca coating improves CO_2 adsorption energy and storage on $C_{24}N_{24}$. First, consider CO_2 molecule adsorption on the single Ca atom coated $C_{24}N_{24}$. Fig. 2c depicts the most stable geometry for CO_2 adsorption on $CaC_{24}N_{24}$. Table 1 shows the associated adsorption energy (E_{ads}), net charge transfer (Q_{CT}) and Hirshfeld charge on the Ca atom (Q_{Ca}). The CO_2 molecule is end-on on $CaC_{24}N_{24}$, with one of its O facing the Ca atom. The binding distance between the O atom of CO_2 and Ca is 2.56 Å, and the associated adsorption energy is −0.48 eV. This low adsorption energy implies that the formed CO_2@$CaC_{24}N_{24}$ complex is stable and that CO_2 adsorption on $CaC_{24}N_{24}$ would be reversible. The adsorbed CO_2 molecule, according to the Hirshfeld analysis, serves as a Lewis base since it supplies 0.17|*e*| to the nanocage. This is followed by a reduction in the atomic charge of the Ca from 0.74|*e*| in the bare $CaC_{24}N_{24}$ to 0.61|*e*| in the CO_2@$CaC_{24}N_{24}$. This means that the transferred charge from CO_2 is primarily concentrated on the Ca atom. Despite this, the EDD map in Fig. 2c indicates that the positively charged Ca atom polarizes the electron density on the interacting O atom of CO_2, as indicated by a significant electron density gain region (pink color). According to the PDOS analysis, the highest occupied molecular orbital (HOMO) of CO_2 is substantially coupled with the electronic states of Ca atom below the Fermi level, confirming our claim that CO_2 acts as a Lewis base on $CaC_{24}N_{24}$.

Table 1 Calculated average adsorption energy (E_{ads}, eV), binding distance (R_{Ca-O}, Å), net charge-transfer (Q_{CT}, electrons), Hirshfeld atomic charge on the Ca atom (Q_{Ca}, |*e*|) of CO_2 adsorbed configurations and the electron density (ρ_{BCP}, a.u.), its Laplacian ($\nabla^2\rho_{BCP}$, a.u.) and total electronic energy density (H_{BCP}, a.u.) at the Ca···OCO BCPs

Complex	E_{ads}	R_{Ca-O}	Q_{CT}[a]	Q_{Ca}	ρ_{BCP}	$\nabla^2\rho_{BCP}$	H_{BCP}
$1CO_2$@$CaC_{24}N_{24}$	−0.48	2.56	0.17	0.61	0.020	0.095	0.003
$2CO_2$@$CaC_{24}N_{24}$	−0.47	2.58	0.15	0.51	0.019	0.093	0.003
$3CO_2$@$CaC_{24}N_{24}$	−0.45	2.59	0.13	0.40	0.018	0.088	0.003
$4CO_2$@$CaC_{24}N_{24}$	−0.42	2.65	0.12	0.37	0.015	0.072	0.003
$5CO_2$@$CaC_{24}N_{24}$	−0.40	2.76	0.10	0.36	0.013	0.060	0.002
$24CO_2$@$Ca_6C_{24}N_{24}$	−0.40	2.73	0.02	0.39	0.014	0.063	0.002

[a] The $Q_{CT} > 0$ values show charge transfer from the CO_2 to nanocage.

To determine the maximum adsorption capacity of $CaC_{24}N_{24}$, more CO_2 molecules are introduced to this cluster until saturation is reached. The relaxed structures of two, three, four and five CO_2 molecules attached on the Ca atom of $CaC_{24}N_{24}$ are shown in Fig. 4. It is seen that all the newly added CO_2 molecules adopt an end-on configuration on the Ca atom, but the corresponding average binding distance between the CO_2 molecules and Ca atom becomes larger and larger as the number of the CO_2 molecules increases (Table 1). Accordingly, the adsorption energy per CO_2 molecule in $2CO_2$@$CaC_{24}N_{24}$, $3CO_2$@$CaC_{24}N_{24}$, $4CO_2$@$CaC_{24}N_{24}$ and $5CO_2$@$CaC_{24}N_{24}$ complexes is −0.47, −0.45, −0.42 and −0.40 eV, respectively. It is worth noting that the amount of change in adsorption energies caused by successive addition of CO_2 molecules on $CaC_{24}N_{24}$ is less than that seen on CaC_{60}.[60] The reasons for the latter observation will be addressed latter. The average charge-transfer value and atomic charge on the Ca atoms also become smaller as the number of the CO_2 molecules increases on the $CaC_{24}N_{24}$ cluster. Since CO_2 molecules are positively charged as a result of donating electrons to the cluster, they repel each other, resulting in decreasing E_{ads} and Q_{CT} values as the number of CO_2 molecules increases. Furthermore, the average Hirshfeld charge on the Ca atom decreases progressively due to CO_2 molecules addition. When the sixth CO_2 molecule is added, we found that the average E_{ads} value of CO_2 molecule decreased to −0.33 eV, indicating that the maximum capacity for the adsorption of CO_2 molecule on $CaC_{24}N_{24}$ is five.

Based on these findings, we allowed five CO_2 molecules to adsorb on each Ca atom of $Ca_6C_{24}N_{24}$. Following the geometry optimizations, we found that each Ca atom of $Ca_6C_{24}N_{24}$ can adsorb up to four CO_2 molecules. According to Table 1, the E_{ads} value per CO_2 molecule in the resulting 24@$Ca_6C_{24}N_{24}$ complexes is −0.40 eV, which is 17% less than the E_{ads} value of a CO_2 value on Ca@$C_{24}N_{24}$. The average charge-transfer value from $Ca_6C_{24}N_{24}$ to CO_2 molecules is 0.08|*e*|, indicating that CO_2

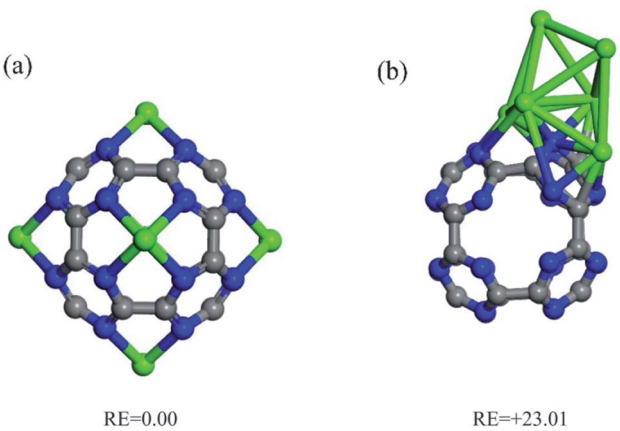

Fig. 3 Two stable isomers and correspond relative energy (RE, in eV) of $Ca_6C_{24}N_{24}$: (a) Ca atoms are disperse on N_4 cavities of $C_{24}N_{24}$ and (b) Ca atoms form a Ca_6 cluster on $C_{24}N_{24}$.

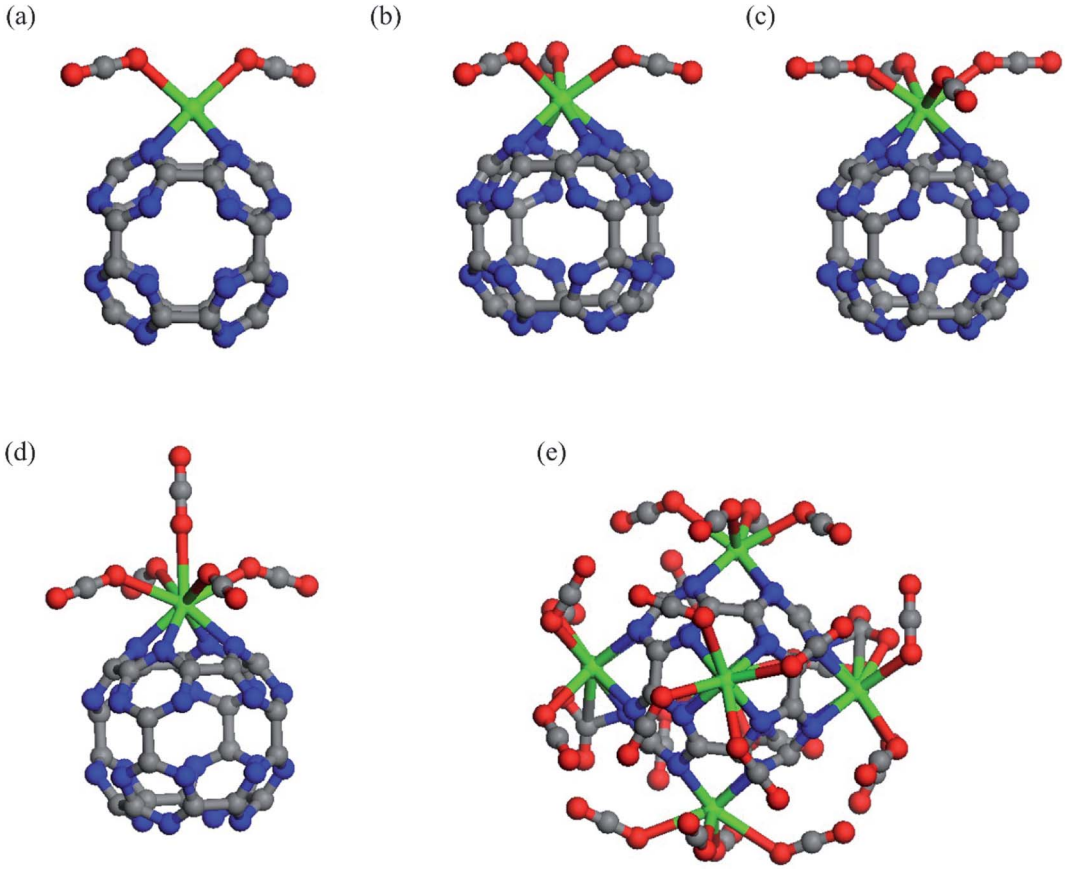

Fig. 4 The optimized structure of the most stable configuration of (a) $2CO_2@CaC_{24}N_{24}$, (b) $3CO_2@CaC_{24}N_{24}$, (c) $4CO_2@CaC_{24}N_{24}$, (d) $5CO_2@CaC_{24}N_{24}$ and (e) $24CO_2@Ca_6C_{24}N_{24}$ complexes. The color code of the atoms: Ca (green); O (red); C (gray); N (blue).

molecules are activated on this cluster. Furthermore, the average E_{ads} value of a CO_2 molecule in the obtained $24@Ca6C_{24}N_{24}$ (−0.40 eV) is within the range suggested for an ideal CO_2 adsorbent (from −0.40 to −0.80 eV).[73]

3.3. Nature of Ca···CO_2 interactions

Further information on the nature of the Ca···CO_2 interactions may be gained by topological analysis of the electron density. The calculated ρ_{BCP}, $\nabla^2\rho_{BCP}$ and H_{BCP} values at the Ca···CO_2 BCPs of different CO_2 adsorbed complexes are listed in Table 1. Fig. S2† depicts the corresponding molecular graphs. The ρ_{BCP} values for all examined systems are small, indicating that the Ca···CO_2 interactions in these systems are moderate. For the $CaC_{24}N_{24}$ fullerene, the tendency of electrons to localize at the Ca···CO_2 BCPs decreases as the number of CO_2 molecules on the Ca atom increases. For example, the average ρ_{BCP} value at the Ca···CO_2 BCPs of $5CO_2@CaC_{24}N_{24}$ is 0.013 a.u., which is about 30% less than the value at $1CO_2@CaC_{24}N_{24}$. Given the linear relationship between bond strengths and ρ_{BCP} values at respective BCP,[77] the Ca···CO_2 interactions weaken as the number of CO_2 molecules on the Ca atom increases. Remarkably, the molecular graphs of the complexes $4CO_2@CaC_{24}N_{24}$ and $5CO_2@CaC_{24}N_{24}$ exhibit BCPs between the C atoms of CO_2 molecules and the C atoms of the fullerene, implying the formation of side interactions in these systems (Fig. S2†). This explains why the average adsorption energy of these systems decreases slowly as the number of CO_2 molecules increases.

The $\nabla^2\rho_{BCP}$ and H_{BCP} values at the Ca···CO_2 BCPs are positive in all complexes studied, indicating that CO_2 adsorption is mainly mediated by electrostatic effects. This finding is explained by the coulombic interaction of positively charged Ca atoms and negative O atom in CO_2. However, when the number of CO_2 molecules increases over the Ca atom, the $\nabla^2\rho_{BCP}$ and H_{BCP} values decrease, suggesting that the contribution of electrostatic interactions in these systems are decreasing.

3.4. Selectivity

In addition to high capacity, a CO_2 storage material should have high selectivity in order to separate CO_2 molecules from other gases such as CH_4, H_2 and N_2 present in natural gas or flue gas mixtures. So, in order to assess the selectivity of the Ca coated $C_{24}N_{24}$ cluster, we investigated the adsorption properties of CH_4, H_2, and N_2 molecules. Fig. 5 depicts the most stable geometries of these molecules on $CaC_{24}N_{24}$, as well as their associated binding distances. Table 2 also summarizes the E_{ads} and Q_{CT} values of these molecules. According to the results, all of the CH_4, H_2, and N_2 molecules are weakly bound to the $CaC_{24}N_{24}$, as shown by their low E_{ads} and Q_{CT} values. This

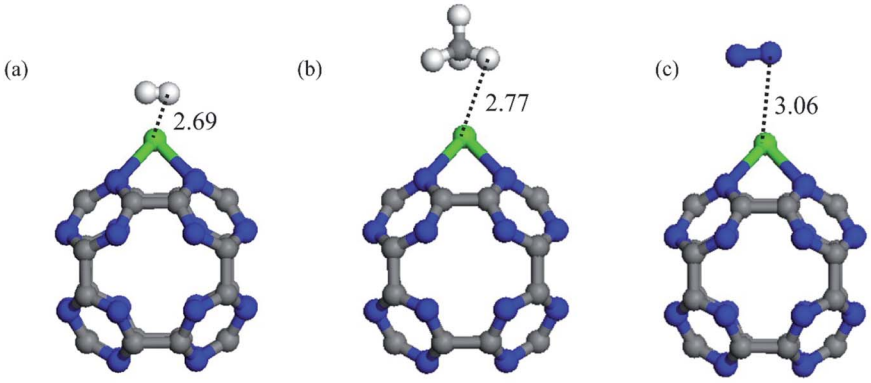

Fig. 5 The optimized structure and relevant bond distances (in Å) of the most stable configuration of (a) H_2, (b) CH_4 and (c) N_2 adsorbed on $CaC_{24}N_{24}$.

Table 2 Calculated adsorption energy (E_{ads}, eV), net charge-transfer (Q_{CT}, electrons) and Hirshfeld atomic charge on the Ca atom (Q_{Ca}, |e|) of H_2, CH_4 and N_2 molecules adsorbed on $CaC_{24}N_{24}$

Complex	E_{ads}	Q_{CT}[a]	Q_{Ca}
H_2@$CaC_{24}N_{24}$	−0.14	0.08	0.67
CH_4@$CaC_{24}N_{24}$	−0.34	0.17	0.60
N_2@$CaC_{24}N_{24}$	−0.07	0.09	0.62

[a] The $Q_{CT} > 0$ values show charge transfer from the CO_2 to nanocage.

means that when the Ca coated $C_{24}N_{24}$ is exposed to CO_2/H_2, CO_2/CH_4 and CO_2/N_2 mixtures, the CO_2 molecules are preferentially adsorbed on the Ca atoms. As a result, Ca coated $C_{24}N_{24}$ can be considered as a selective adsorbent for CO_2 separation from the aforementioned gas mixtures.

4. Conclusions

To summarize, the effect of Ca coating on the CO_2 adsorption behaviors of porphyrin-like porous fullerene ($C_{24}N_{24}$) was thoroughly studied using the DFT calculations. A CO_2 molecule may be reversibly adsorbed on Ca coated $C_{24}N_{24}$ with an adsorption energy of −0.48 eV, as opposed to bare $C_{24}N_{24}$. The Ca atoms are located on the center of the N_4 cavity of $C_{24}N_{24}$ due to strong electrostatic interactions as well as charge transfer from the Ca atoms to the fullerene. Ca atoms do not aggregate and cluster on $C_{24}N_{24}$ because to the strong Ca–N interactions. Each Ca atom in the fully coated $Ca_6C_{24}N_{24}$ fullerene may adsorb up to four CO_2 molecules with an E_{ads} value of −0.40 eV per CO_2. This is within the recommended range for an ideal CO_2 storage material. Furthermore, Ca coated $C_{24}N_{24}$ has a high potential for separating CO_2 gas from flue gas or natural gas mixtures. These findings might inspire intensive experimental attempts to develop high-efficiency CO_2 storage media.

Conflicts of interest

There are no conflicts to declare.

References

1 H. W. Kroto, J. R. Heath, S. C. O'Brien, R. F. Curl and R. E. Smalley, *Nature*, 1985, **318**, 162–163.
2 S. Iijima and T. Ichihashi, *Nature*, 1993, **363**, 603–605.
3 S. Iijima, *Phys. B*, 2002, **323**, 1–5.
4 K. S. Novoselov, A. K. Geim, S. V. Morozov, D.-e. Jiang, Y. Zhang, S. V. Dubonos, I. V. Grigorieva and A. A. Firsov, *Science*, 2004, **306**, 666–669.
5 C. Berger, Z. Song, T. Li, X. Li, A. Y. Ogbazghi, R. Feng, Z. Dai, A. N. Marchenkov, E. H. Conrad and P. N. First, *J. Phys. Chem. B*, 2004, **108**, 19912–19916.
6 A. E. Mahdy, *Mol. Phys.*, 2015, **113**, 3531–3544.
7 C. Ramos-Castillo, J. Reveles, R. Zope and R. De Coss, *J. Phys. Chem. C*, 2015, **119**, 8402–8409.
8 C. Ramos-Castillo, J. Reveles, M. Cifuentes-Quintal, R. Zope and R. de Coss, *J. Phys. Chem. C*, 2016, **120**, 5001–5009.
9 F. Bottacchi, L. Petti, F. Späth, I. Namal, G. Tröster, T. Hertel and T. D. Anthopoulos, *Appl. Phys. Lett.*, 2015, **106**, 51–52.
10 X. Wang, G. Li, G. Hong, Q. Guo and X. Zhang, *ACS Appl. Mater. Interfaces*, 2017, **9**, 41323–41331.
11 T. Ye, Y. Sun, X. Zhao, B. Lin, H. Yang, X. Zhang and L. Guo, *J. Mater. Chem. A*, 2018, **6**, 18994–19003.
12 L. Bai, Y. Lei, H. Huang and Y. Xiang, *ACS Appl. Mater. Interfaces*, 2020, **12**, 33139–33151.
13 P. Su, K. Iwase, S. Nakanishi, K. Hashimoto and K. Kamiya, *Small*, 2016, **12**, 6083–6089.
14 I. H. Lin, Y. H. Lu and H. T. Chen, *J. Comput. Chem.*, 2017, **38**, 2041–2046.
15 M. D. Esrafili, *Chem. Phys. Lett.*, 2018, **705**, 44–49.
16 Y. Zhang, D. Zhang and C. Liu, *J. Phys. Chem. B*, 2006, **110**, 4671–4674.
17 Y. Chen, B. Gao, J.-X. Zhao, Q.-H. Cai and H.-G. Fu, *J. Mol. Model.*, 2012, **18**, 2043–2054.
18 J. N. Gavgani, A. Hasani, M. Nouri, M. Mahyari and A. Salehi, *Sens. Actuators, B*, 2016, **229**, 239–248.
19 L.-F. Velázquez-López, S.-M. Pacheco-Ortin, R. Mejía-Olvera and E. Agacino-Valdés, *J. Mol. Model.*, 2019, **25**, 1–11.
20 L. Ferrighi, M. I. Trioni and C. Di Valentin, *J. Phys. Chem. C*, 2015, **119**, 6056–6064.

21 H. Miao, S. Li, Z. Wang, S. Sun, M. Kuang, Z. Liu and J. Yuan, *Int. J. Hydrogen Energy*, 2017, **42**, 28298–28308.
22 M. D. Esrafili and S. Asadollahi, *Appl. Surf. Sci.*, 2018, **463**, 526–534.
23 P. Sun, H. Liu, M. Feng, Z. Zhai, Y. Fang, X. Zhang and V. K. Sharma, *Appl. Catal., B*, 2020, **272**, 119005.
24 J. Guo, S. Zhang, M. Zheng, J. Tang, L. Liu, J. Chen and X. Wang, *Int. J. Hydrogen Energy*, 2020, **45**, 32402–32412.
25 X. Zhang, Z. Lu and Z. Yang, *J. Mol. Catal. A: Chem.*, 2016, **417**, 28–35.
26 M. Wang and Z. Wang, *RSC Adv.*, 2017, **7**, 48819–48824.
27 X. Zhang, X. Xie, H. Wang, J. Zhang, B. Pan and Y. Xie, *J. Am. Chem. Soc.*, 2013, **135**, 18–21.
28 Z. Jin and L. Zhang, *J. Mater. Sci. Technol.*, 2020, **49**, 144–156.
29 V. Tripkovic, M. Vanin, M. Karamad, M. r. E. Björketun, K. W. Jacobsen, K. S. Thygesen and J. Rossmeisl, *J. Phys. Chem. C*, 2013, **117**, 9187–9195.
30 Z. Wang, J. Zhao and Q. Cai, *Phys. Chem. Chem. Phys.*, 2017, **19**, 23113–23121.
31 E. Ashori, F. Nazari and F. Illas, *Phys. Chem. Chem. Phys.*, 2017, **19**, 3201–3213.
32 D. H. Lee, W. J. Lee, W. J. Lee, S. O. Kim and Y.-H. Kim, *Phys. Rev. Lett.*, 2011, **106**, 175502.
33 J. Zeng and K.-Q. Chen, *Appl. Phys. Lett.*, 2014, **104**, 033104.
34 H. Hamadi, E. Shakerzadeh and M. D. Esrafili, *Chem. Phys. Lett.*, 2019, **724**, 80–85.
35 E. Shakerzadeh, H. Hamadi and M. D. Esrafili, *Inorg. Chem. Commun.*, 2019, **106**, 190–196.
36 K. Srinivasu and S. K. Ghosh, *J. Phys. Chem. C*, 2012, **116**, 25184–25189.
37 M. D. Esrafili and B. Nejadebrahimi, *Chem. Phys. Lett.*, 2019, **716**, 11–16.
38 B. Modak, K. Srinivasu and S. K. Ghosh, *Int. J. Hydrogen Energy*, 2017, **42**, 2278–2287.
39 M. D. Esrafili and H. Hamadi, *Mol. Phys.*, 2020, **118**, e1797919.
40 A. Tatar, A. Barati-Harooni, A. Najafi-Marghmaleki, A. Mohebbi, M. M. Ghiasi, A. H. Mohammadi and A. Hajinezhad, *Int. J. Greenhouse Gas Control*, 2016, **53**, 85–972016.
41 I. G. Wilson and I. Staffell, *Nat. Energy*, 2018, **3**, 365–372.
42 T. Montanari, E. Finocchio, E. Salvatore, G. Garuti, A. Giordano, C. Pistarino and G. Busca, *Energy*, 2011, **36**, 314–319.
43 J. O. Abe, A. Popoola, E. Ajenifuja and O. Popoola, *Int. J. Hydrogen Energy*, 2019, **44**, 15072–15086.
44 J. Bradshaw, S. Bachu, D. Bonijoly, R. Burruss, S. Holloway, N. P. Christensen and O. M. Mathiassen, *Int. J. Greenhouse Gas Control*, 2007, **1**, 62–68.
45 F. D. Meylan, V. Moreau and S. Erkman, *J. CO_2 Util.*, 2015, **12**, 101–108.
46 M. S. Duyar, S. Wang, M. A. Arellano-Trevino and R. J. Farrauto, *J. CO_2 Util.*, 2016, **15**, 65–71.
47 P. Kelemen, S. M. Benson, H. Pilorgé, P. Psarras and J. Wilcox, *Front. Clim.*, 2019, **1**, 9.
48 F. Su, C. Lu, S.-C. Kuo and W. Zeng, *Energy Fuels*, 2010, **24**, 1441–1448.
49 S. Kumar, R. Srivastava and J. Koh, *J. CO_2 Util.*, 2020, **41**, 101251.
50 R. Babarao and J. Jiang, *Energy Environ. Sci.*, 2008, **1**, 139–143.
51 Y. Zeng, R. Zou and Y. Zhao, *Adv. Mater.*, 2016, **28**, 2855–2873.
52 W. Leitner, *Coord. Chem. Rev.*, 1996, **153**, 257–284.
53 G. Qin, Q. Cui, W. Wang, P. Li, A. Du and Q. Sun, *ChemPhysChem*, 2018, **19**, 2788–2795.
54 N. Sathishkumar, S.-Y. Wu and H.-T. Chen, *Chem. Eng. J.*, 2020, **391**, 123577.
55 A. Liu, J. Long, S. Yuan, W. Cen and J. Li, *Phys. Chem. Chem. Phys.*, 2019, **21**, 5133–5141.
56 C. Chen, K. Xu, X. Ji, L. Miao and J. Jiang, *Phys. Chem. Chem. Phys.*, 2014, **16**, 11031–11036.
57 M. D. Esrafili, *J. Mol. Graphics Modell.*, 2019, **90**, 192–198.
58 N. Sathishkumar, S.-Y. Wu and H.-T. Chen, *Chem. Eng. J.*, 2021, **407**, 127194.
59 C. He, R. Wang, D. Xiang, X. Li, L. Fu, Z. Jian, J. Huo and S. Li, *Appl. Surf. Sci.*, 2020, **509**, 145392.
60 B. Gao, J.-x. Zhao, Q.-h. Cai, X.-g. Wang and X.-z. Wang, *J. Phys. Chem. A*, 2011, **115**, 9969–9976.
61 G. Gao, F. Ma, Y. Jiao, Q. Sun, Y. Jiao, E. Waclawik and A. Du, *Comput. Mater. Sci.*, 2015, **108**, 38–41.
62 J. P. Perdew, K. Burke and M. Ernzerhof, *Phys. Rev. Lett.*, 1996, **77**, 3865–3868.
63 B. Delley, *J. Chem. Phys.*, 1990, **92**, 508–517.
64 B. Delley, *J. Chem. Phys.*, 2000, **113**, 7756–7764.
65 S. Grimme, *J. Comput. Chem.*, 2006, **27**, 1787–1799.
66 R. Bader, *Atoms in Molecules: A Quantum Theory*, Clarendon Press, Oxford, 1990.
67 I. Rozas, I. Alkorta and J. Elguero, *J. Am. Chem. Soc.*, 2000, **122**, 11154–11161.
68 M. Frisch, G. Trucks, H. Schlegel, G. Scuseria, M. Robb, J. Cheeseman, G. Scalmani, V. Barone, B. Mennucci and G. Petersson, Gaussian Inc., Wallingford CT, 2009.
69 F. Biegler-König and J. Schönbohm, *J. Comput. Chem.*, 2002, **23**, 1489–1494.
70 E. Shakerzadeh, Z. Mashak Shabavi and E. C. Anota, *Appl. Organomet. Chem.*, 2020, **34**, e5694.
71 Q. Sun, M. Wang, Z. Li, A. Du and D. J. Searles, *J. Phys. Chem. C*, 2014, **118**, 2170–2177.
72 H. Dong, B. Lin, K. Gilmore, T. Hou, S.-T. Lee and Y. Li, *Curr. Appl. Phys.*, 2015, **15**, 1084–1089.
73 S. Chu and A. Majumdar, *Nature*, 2012, **488**, 294.
74 D. C. Camacho-Mojica, E. Muñoz-Sandoval and F. López-Urías, *Carbon*, 2017, **116**, 381–390.
75 E. Shakerzadeh, H. Hamadi and M. D. Esrafili, *Inorg. Chem. Commun.*, 2019, **106**, 190–196.
76 P. Mousavian and M. D. Esrafili, *Inorg. Chem. Commun.*, 2020, **122**, 108317.
77 M. A. Spackman, *Cryst. Growth Des.*, 2015, **15**, 5624–5628.